GEOPHYSICS, VOL. 78, NO. 2 (MARCH-APRIL 2013); P. N1–N10, 9 FIGS., 1 TABLE.
10.1190/GEO2012-0319.1

Seismic characterization of reservoirs with asymmetric fractures

Mehdi E. Far[1], Leon Thomsen[2], and Colin M. Sayers[3]

ABSTRACT

Variations of reflection amplitude with offset and azimuth are sensitive to the presence of natural and induced fractures. We tested inversion for fracture compliance matrix components from wide azimuth noisy synthetic PP-reflection data. The model was a fractured reservoir with monoclinic symmetry, formed by two sets of vertical asymmetric fractures embedded in a VTI background. The fractures (joints) were assumed to be vertical, with noncircular shape and/or with asymmetric shear compliance. Results of synthetic inversion showed that an incorrect assumption about fracture shear symmetry (e.g., treating asymmetric fractures as rotationally invariant fractures) can cause considerable error in estimation of the fracture compliance matrix. Components of effective second- and fourth-rank fracture compliance matrices for a medium with monoclinic symmetry (which takes into account layering and multiple fracture sets) can be used as attributes related to the characteristics of the fractured medium. Monte Carlo simulation was used to test the effect of uncertainties in the a priori information (about background VTI parameters of unfractured rock), as they affect inversion for these attributes. According to this analysis, the direction of fast shear-wave polarization was inverted robustly in the Monte Carlo simulation. Although the average values of the components of fracture compliance matrices obtained from Monte Carlo simulation were in agreement with the actual values used for forward modeling, individual values obtained in Monte Carlo simulation were sensitive to uncertainties in the background properties in general. Because the elastic properties of background VTI media without fractures (or other azimuthally variable features) do not cause azimuthal changes in reflection coefficient variation with offset, simultaneous inversion for background properties and fracture tensor components require additional constraints.

INTRODUCTION

Fractures usually show preferred orientations that may result in significant permeability anisotropy in the reservoir. Thus it is important for optimum drainage that the separation of producing wells should be more closely spaced along the direction of minimum permeability than along the direction of maximum permeability (Sayers, 2010). This work studies the feasibility of determining these preferred directions using seismic data.

In the presence of oriented sets of fractures, seismic wave velocities and reflection amplitudes vary with offset and azimuth. Seismic velocity anisotropy can be caused by different factors, such as rock fabric, grain-scale microcracks, rock layering, and aligned fractures at all scales, provided that the characteristic dimensions of these features are small relative to the seismic wavelength (Worthington, 2008). Reflection amplitudes have higher vertical resolution and are more sensitive to the properties of the reservoir, compared to velocities. Therefore, they have advantages over seismic velocities for characterizing fractured reservoirs. Sil et al. (2011) also discuss the advantages of using seismic amplitudes over seismic velocities. Lynn et al. (1994) use P-wave amplitude variation with offset and azimuth (AVOA) data to characterize fractured reservoirs, using a simple model for the fractures. In this paper, AVOA is used to invert for the components of the fracture compliance matrices, while allowing for more complex fracturing. These matrices capture the effect of variable fracture orientation and density, specific compliance, the most compliant direction in the reservoir (Helbig, 1994; Sayers, 2009), and fracture interactions.

Manuscript received by the Editor 12 August 2012; revised manuscript received 6 October 2012; published online 5 February 2013.
[1]University of Houston, Department of Earth and Atmospheric Sciences, Houston, Texas, USA. E-mail: meftekhari@gmail.com.
[2]University of Houston, Department of Earth and Atmospheric Sciences, Houston, Texas, USA, and Delta Geophysics, Houston, Texas, USA. E-mail: lathomse@mail.uh.edu.
[3]University of Houston, Department of Earth and Atmospheric Sciences, Houston, Texas, USA, and Schlumberger, Houston, Texas, USA. E-mail: csayers@slb.com.

Far (2011), Far et al. (2012), and Eftekharifar and Sayers (2011a, 2011b), among many others, demonstrate the use of synthetic AVOA data and resolution matrix for the characterization of fractured reservoirs with "symmetric fractures," i.e., fractures with rotationally invariant shear compliance. For such fractures, it is assumed that the specific shear compliance of the fractures is rotationally invariant around the normal to the fractures. The theory of Sayers and Kachanov (Kachanov, 1980; Sayers and Kachanov, 1991; Sayers and Kachanov, 1995) is used for effective medium modeling of media with rotationally invariant fractures. This work extends the previous work to the case of asymmetric fractures.

Previous models used to invert the seismic response of fractured reservoirs often assume a single set of aligned fractures with horizontally transverse isotropic (HTI) symmetry (e.g., Mallick et al., 1996; Rüger, 1997; Sayers and Rickett, 1997), whereas most reservoirs contain several sets of fractures with variable orientation within a given fracture set (see, e.g., Sayers, 1998; Bakulin et al., 2000; Sayers and Dean, 2001; Far, 2011). The use of simplified models such as HTI can be misleading (see, e.g., Far, 2011; Far et al., 2012).

Results of this study show the importance of our assumptions about fracture shape and the consequences of considering simplified models for fractures. Results show that knowledge of background unfractured rock properties is crucial for accurate inversion of fracture parameters. Optimization of seismic survey design is demonstrated using singular value decomposition and inversion of synthetic AVOA data (see Far, 2011; Eftekharifar and Sayers, 2011a, 2011b; Far et al., 2012). Synthetic AVOA data for an arbitrary number of differently oriented vertical fractures can be analyzed to identify which well-resolved parameter combinations can be determined for various experimental geometries.

THEORY

According to linear slip theory (e.g., Schoenberg, 1980), the small vector difference across a fracture, in the displacement, is assumed to depend linearly on the traction vector (Jones and Whittier, 1967; Schoenberg, 1980). For a vertical fracture surface within an elastic medium, we assume a coordinate system with x_1 and x_3 in directions tangential to the local fracture plane and x_2 perpendicular to that fracture plane. Let $\mathbf{u}$ denote displacement (see Figure 1a), and let

$$\Delta\mathbf{u} = \mathbf{u}^R - \mathbf{u}^L \tag{1}$$

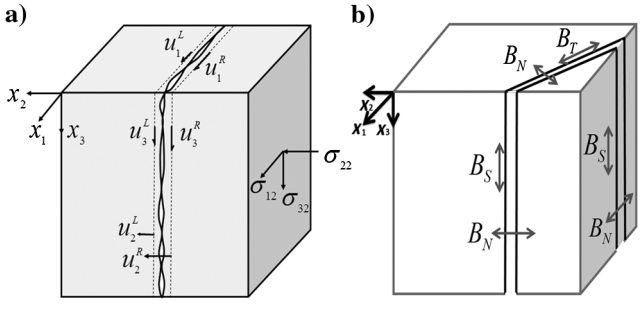

Figure 1. (a) The normal and tangential displacements at the face of the fracture are denoted by u_3, u_1, and u_2. The normal and tangential components of the displacement discontinuity at the fracture are given by $\Delta u_i = u_i^R - u_i^L$ and are related to the normal and shear tractions. (b) Vertical asymmetric fractures.

denote the difference or discontinuity of displacement between the right (R) fracture face and left (L) fracture face. The time dependency is suppressed. The traction vector $\mathbf{t}$ we take as the second row of the stress tensor, with components τ_{21}, τ_{22}, and τ_{23}, which are the forces per unit area that the material on the right side of the interface exerts on the left side. In index notation,

$$\Delta u_i = B_{ij} t_j. \tag{2}$$

If there is no rotational symmetry around the normal x_2 to the fracture (e.g., due to different fracture dimensions in different directions and/or slickensides, striations, or "microcorrugation" [Bakulin et al., 2000]), one can define the fracture shear compliances B_T and B_S (T for transverse; S for shear) in two principal directions (assumed here to be x_1 and x_3), and also normal compliance B_N in the direction perpendicular to the fracture plane (see Figure 1b).

For fully asymmetric fractures, the $\mathbf{B}$ tensor is written as

$$\mathbf{B} = \begin{bmatrix} B_T & 0 & B_{13} \\ 0 & B_N & 0 \\ B_{13} & 0 & B_S \end{bmatrix}. \tag{3}$$

For the vertical fractures considered in this work, we further assume that the fractures have a horizontal mirror symmetry plane perpendicular to x_3 (the vertical direction). These assumptions include joints, elongated in the one-direction, and exclude cracks that are striated at angles other than 0° or 90°. These assumptions seem to be reasonable in contexts in which the maximum principal stress is vertical, and the failure is of Type I (extension). They restrict the generality of the following, but they include a large class of noncircular cracks; we refer to these below as "asymmetrical fractures." The matrix $\mathbf{B}$ then becomes

$$\mathbf{B} = \begin{bmatrix} B_T & 0 & 0 \\ 0 & B_N & 0 \\ 0 & 0 & B_S \end{bmatrix}. \tag{4}$$

If the asymmetry comes from the overall crack shape (e.g., ribbon-shaped joints rather than penny-shaped cracks), intuitively these horizontal excess specific compliances B_T will be larger than the corresponding vertical parameters B_S. Worthington (2008) shows that fracture specific compliances are related to fracture dimension.

As one example, Margetan et al. (1988) model a set of fractures consisting of regular arrays of thin striplike cracks embedded in a background medium with Poisson's ratio ν, as shown in Figure 2; the width of the cracks is assumed to be small compared to the wavelength. Using the results tabulated by Tada et al. (1973), Margetan et al. (1988) find that for a periodic array of strip cracks with shear traction parallel to the long axis of the cracks (ν is the Poisson ratio of the homogeneous background medium)

$$B_N/B_T = 1 - \nu, \tag{5}$$

whereas for traction perpendicular to the long axis of the cracks,

$$B_N/B_S = 1. \tag{6}$$

As a result, a fracture modeled as a periodic array of strip cracks will display anisotropy of the shear compliance in the plane of the fracture with

$$B_S/B_T = 1 - \nu. \tag{7}$$

This model is not really indicative of a set of joints, which are repeated in the x_2 direction, rather than the x_3 direction, but it indicates the sort of variation that we might expect.

In another model, an elliptically shaped fracture in an isotropic background with normal **n** and principal axes **s** and **t** in the plane of the fracture, the fracture compliance matrix can be written (Kachanov, 1992) as

$$\mathbf{B} = B_N \mathbf{nn} + B_S \mathbf{ss} + B_T \mathbf{tt}, \tag{8}$$

where

$$B_N = \frac{8(1-\nu^2)}{3E(k)} \frac{\pi a b^2}{E(k)} = \frac{32(1-\nu^2)S^2}{3\pi E(k) P}, \tag{9}$$

where $P = 4aE(k)$ and $S = \pi ab$ are the perimeter and area of the ellipse, and $E(k)$ is the complete elliptic integral of the first kind, with argument $k = [1-(b/a)]^{1/2}$ (Budiansky and O'Connell, 1976; Sevostianov and Kachanov, 2002). Here, B_T and B_S are obtained from B_N by replacing $E(k)$ by Q and R, respectively, where

$$Q(k,\nu) = k^{-2}[(k^2+\nu-\nu k^2)E(k) - \nu(1-k^2)K(k)], \tag{10}$$

$$R(k,\nu) = k^{-2}[(k^2-\nu)E(k) + \nu(1-k^2)K(k)], \tag{11}$$

where $K(k)$ is the complete elliptic integral of the second kind (Budiansky and O'Connell, 1976; Sevostianov and Kachanov, 2002). Hence, we have

$$B_T/B_S = Q(k,\nu)/R(k,\nu). \tag{12}$$

Figure 3 shows a plot of B_T/B_S for elliptical cracks for different aspect ratios b/a, where b is the minor and a is the major axis in the plane of the crack, for various values of the Poisson's ratio of the background medium, assumed isotropic. When $a = b$, $B_T = B_S$ as expected, but as b/a decreases, B_T becomes more compliant than B_S. As $b/a \to 0$, $B_S/B_T \to 1-\nu$, the limit for strip cracks given by equation 7. This effect is particularly significant for carbonate or shale reservoirs for which Poisson's ratios in the range greater than 0.25 are not uncommon.

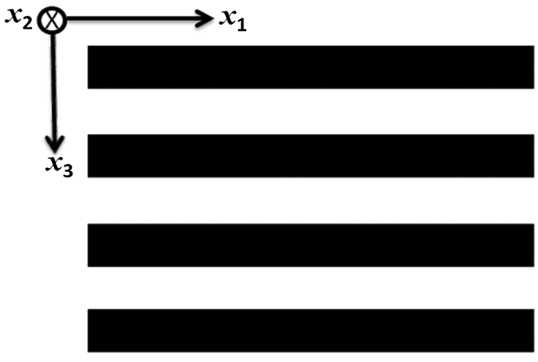

Figure 2. Margetan et al. (1988) consider interfaces consisting of a periodic array of cracks. The shaded regions indicate cracks at the interface, whereas the unshaded regions indicate perfect bonding. The cracks are assumed to be thin in the direction perpendicular to the interface. Note that the cracks are thin in the direction perpendicular to the figure. Therefore, the planes of the cracks are normal to the x_2 direction and therefore parallel to the plane of the figure.

From these models, we conclude that values of $B_S/B_T < 1$, but not $\ll 1$, are plausible, for asymmetric fractures in an isotropic background. We assume that similar values are appropriate for such fractures in a polar anisotropic background.

For a vertical asymmetric fracture with an arbitrary azimuth, **B** can be written in the following compact form (Far, 2011; Far et al., 2012):

$$B_{ij}^{(r)} = B_N^{(r)} n_i n_j + B_T^{(r)}(\delta_{ij} - n_i n_j) + (B_S^{(r)} - B_T^{(r)})\delta_{3i}\delta_{3j}, \tag{13}$$

where n_i ($i = 1, 2, 3$) is the ith component of the vector normal to the fracture plane. In an elastic medium that contains an arbitrary number of sets of fractures with arbitrary orientation distribution, using the divergence theorem and Hooke's law it can be shown (Hill, 1963; Sayers and Kachanov, 1995; Lehner, 2008) that the elastic compliance tensor of the fractured medium can be written in the following form:

$$S_{ijkl} = S^0_{ijkl} + \Delta S_{ijkl}, \tag{14}$$

where $\mathbf{S}^0$ is the compliance matrix of the background medium (including the effects of stress, pores, and cracks, except for those fractures explicitly included in $\Delta\mathbf{S}$, which are treated explicitly here).

Following Nichols et al. (1989), the additional (effective) compliance matrix $\Delta\mathbf{S}$, for Q sets of aligned fractures can be written,

$$\Delta\mathbf{S} = \sum_{q=1}^{Q} \Delta\mathbf{S}^q, \tag{15}$$

where $\Delta\mathbf{S}^q$ is the effective fracture compliance matrix of the qth set of aligned fractures. Implicitly, each of these effective fracture compliances depends upon the rest of the microgeometry, specifically including the presence, location, size, and orientation of the other fractures (including their intersections, if liquid filled).

Defining effective normal and shear compliances (Sayers and Kachanov, 1995; Sayers, 2010) and following the same logic as described therein for rotationally invariant fractures, one finds

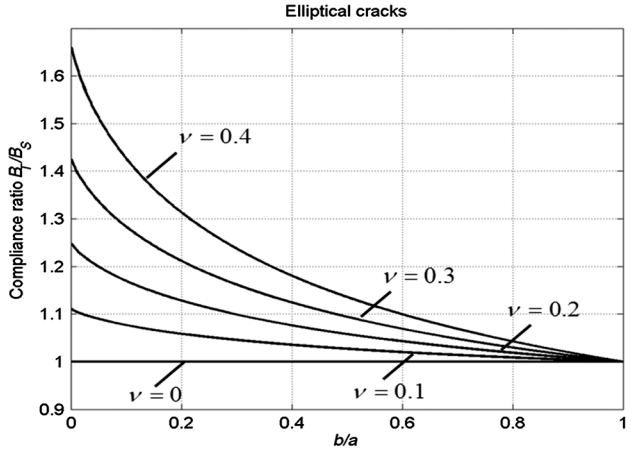

Figure 3. Plot of B_T/B_S for elliptical cracks for different aspect ratios b/a, where b is the minor axis and a is the major axis in the plane of the crack, for various values of Poisson's ratio of the background medium, assumed isotropic.

$$\Delta S_{ijkl} = \frac{1}{V}\sum_r \Big[\frac{B_T^{(r)}}{4}(\delta_{ik}n_j^{(r)}n_l^{(r)} + \delta_{il}n_j^{(r)}n_k^{(r)} + \delta_{jk}n_i^{(r)}n_l^{(r)} + \delta_{jl}n_i^{(r)}n_k^{(r)}) + \frac{(B_S^{(r)} - B_T^{(r)})}{4}(\delta_{3i}\delta_{3k}n_j^{(r)}n_l^{(r)} + \delta_{3i}\delta_{3l}n_j^{(r)}n_k^{(r)} + \delta_{3j}\delta_{3k}n_i^{(r)}n_l^{(r)} + \delta_{3j}\delta_{3l}n_i^{(r)}n_k^{(r)}) + (B_N^{(r)} - B_T^{(r)})n_i^{(r)}n_j^{(r)}n_k^{(r)}n_l^{(r)}\Big]A^{(r)}. \quad (16)$$

We recast this as

$$\Delta S_{ijkl} = \frac{1}{4}(\delta_{3i}\delta_{3k}\kappa_{jl} + \delta_{3i}\delta_{3l}\kappa_{jk} + \delta_{3j}\delta_{3k}\kappa_{il} + \delta_{3j}\delta_{3l}\kappa_{ik}) + \frac{1}{4}(\delta_{ik}\alpha_{jl} + \delta_{il}\alpha_{jk} + \delta_{jk}\alpha_{il} + \delta_{jl}\alpha_{ik}) + \beta_{ijkl}, \quad (17)$$

where δ_{ij} is the Kronecker delta and

$$\alpha_{ij} = \frac{1}{V}\sum_r B_T^{(r)}n_i^{(r)}n_j^{(r)}A^{(r)},$$
$$\kappa_{ij} = \frac{1}{V}\sum_r (B_S^{(r)} - B_T^{(r)})n_i^{(r)}n_j^{(r)}A^{(r)},$$
$$\beta_{ijkl} = \frac{1}{V}\sum_r (B_N^{(r)} - B_T^{(r)})n_i^{(r)}n_j^{(r)}n_k^{(r)}n_l^{(r)}A^{(r)}, \quad (18)$$

where the sum is over all fractures in volume V (implicitly including all fracture sets q), $n_i^{(r)}$ is the ith component of the normal to the rth fracture, $A^{(r)}$ is its area, and $B_N^{(r)}$ and $B_{T,S}^{(r)}$ are its normal and shear compliances. The relative magnitude of $\boldsymbol{\kappa}$ shows the degree of asymmetry of the fractures; thus, $\boldsymbol{\kappa}$ will reduce to zero for rotationally invariant fractures. It is assumed here that the background medium (without fractures) is polar isotropic with a vertical axis of rotational symmetry (VTI). In this case, the elastic symmetry of the fractured rock will be monoclinic for an arbitrary number of vertical fractures with different azimuths, although this symmetry reduces to orthotropic in certain simple situations (Far, 2011). The excess compliances ΔS_{ijkl}, resulting from the presence of one or more sets of fractures with arbitrary azimuths are then, in the conventional two-index (Voigt) notation (Far, 2011; Far et al., 2012)

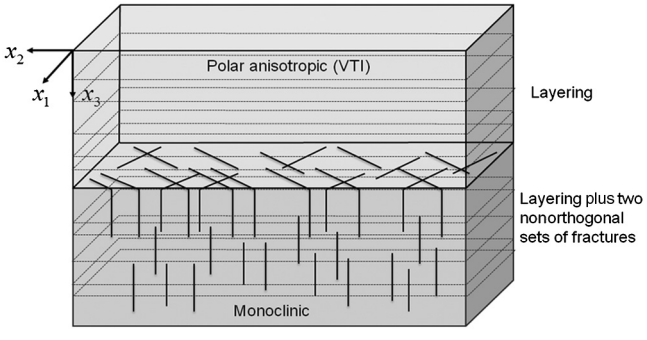

Figure 4. Symmetry types considered for host (overburden) medium (VTI) and reservoir (monoclinic).

$$\Delta\mathbf{S} = \begin{bmatrix} \alpha_{11}+\beta_{1111} & \beta_{1122} & 0 & 0 & 0 & \alpha_{12}+2\beta_{1112} \\ \beta_{1122} & \alpha_{22}+\beta_{2222} & 0 & 0 & 0 & \alpha_{12}+2\beta_{1222} \\ 0 & 0 & 0 & 0 & 0 & 0 \\ 0 & 0 & 0 & \alpha_{22}+\kappa_{22} & \alpha_{12}+\kappa_{12} & 0 \\ 0 & 0 & 0 & \alpha_{12}+\kappa_{12} & \alpha_{11}+\kappa_{11} & 0 \\ \alpha_{12}+2\beta_{1112} & \alpha_{12}+2\beta_{1222} & 0 & 0 & 0 & \alpha_{11}+\alpha_{22}+4\beta_{1122} \end{bmatrix}. \quad (19)$$

Derivations for the more general case of nonvertical fractures are shown in Appendix A. The effective compliance tensor S_{ijkl} can be calculated using equation 14, which can be inverted for the stiffness tensor $\mathbf{C}$, of seismological interest. But, when the excess compliance $\boldsymbol{\Delta S}$ is small, one can directly calculate $\mathbf{C}$ as a perturbation from the background stiffness matrix $\mathbf{C_0}$ (e.g., Sayers, 2009):

$$\mathbf{C} = \mathbf{C_0} - \mathbf{C_0}\,\boldsymbol{\Delta S}\,\mathbf{C_0}. \quad (20)$$

We will use, for the VTI background, $\mathbf{C_0} = \mathbf{C}_{\mathrm{VTI}}$. The direction of the fast vertically propagating shear-wave polarization can be obtained as (Far, 2011; Far et al., 2012)

$$\tan(2\varphi_{S1}) = \frac{2(\alpha_{12}+\kappa_{12})}{\alpha_{11}+\kappa_{11}-\alpha_{22}-\kappa_{22}}. \quad (21)$$

For reflectivity modeling, a two-layer model will be assumed, in which the overburden is assumed to be VTI without fractures, and the underlying medium is assumed to consist of different sets of fractures embedded in a VTI medium (see Figure 4). Further, the anisotropy and contrast between the overburden and reservoir are assumed to be small. In this situation, the P-wave plane-wave reflection coefficient can be written in the following form (Pšenčík and Martins, 2001):

$$R_{PP}(\theta,\phi) = R_{PP}^{\mathrm{iso}}(\theta) + \frac{1}{2}\Delta\varepsilon_z + \frac{1}{2}\Big[\Big(\Delta\delta_x - 8\frac{\bar{V}_S^{\,2}}{\bar{V}_P^{\,2}}\Delta\gamma_x\Big)\cos^2\phi + \Big(\Delta\delta_y - 8\frac{\bar{V}_S^{\,2}}{\bar{V}_P^{\,2}}\Delta\gamma_y\Big)\sin^2\phi + 2\Big(\Delta\chi_z - 4\frac{\bar{V}_S^{\,2}}{\bar{V}_P^{\,2}}\Delta\varepsilon_{45}\Big)\cos\phi\,\sin\phi - \Delta\varepsilon_z\Big]\sin^2\theta + \frac{1}{2}[\Delta\varepsilon_x\cos^4\phi + \Delta\varepsilon_y\sin^4\phi + \Delta\delta_z\cos^2\phi\sin^2\phi + 2(\Delta\varepsilon_{16}\cos^2\phi + \Delta\varepsilon_{26}\sin^2\phi)\cos\phi\,\sin\phi]\sin^2\theta\tan^2\theta, \quad (22)$$

where θ is the polar angle; ϕ is the azimuth (measured with respect to the x_1 axis of an arbitrary coordinate system); $R_{PP}^{\mathrm{iso}}(\theta)$ denotes the weak-contrast reflection coefficient ignoring all anisotropic terms; and $\bar{V}_P = \frac{V_{P01}+V_{P02}}{2}$, $\bar{V}_S = \frac{V_{S01}+V_{S02}}{2}$ are the average properties of the upper and lower media. The differences (in equation 22) across the plane in generalized anisotropic parameters (Thomsen, 1986) are, for example, $\Delta\varepsilon_x = \varepsilon_x^{\mathrm{lower}} - \varepsilon_x^{\mathrm{upper}}$ (Pšenčík and Martins, 2001; Far et al., 2013). In terms of the specific compliance matrices $\boldsymbol{\alpha}$, $\boldsymbol{\kappa}$, $\boldsymbol{\beta}$, these parameters are presented in Appendix B.

Substitution of expressions for the anisotropy parameters in terms of $\boldsymbol{\alpha}$, $\boldsymbol{\kappa}$, $\boldsymbol{\beta}$ into equation 22 allows the "sensitivities" F_{ij} and F_{ijkl} of $R_{PP}(\theta,\phi)$ to α_{ij}, κ_{ij}, and β_{ijkl} to be determined (Far, 2011; Far et al., 2012)

$$R_{PP}(\theta,\phi) = R_{PP}^{\text{iso}}(\theta) + R_{PP}^{\text{aniso}}(\theta) + F_{11}^{\alpha}(\theta,\phi)\alpha_{11} + F_{12}^{\alpha}(\theta,\phi)\alpha_{12} + F_{22}^{\alpha}(\theta,\phi)\alpha_{22} + F_{11}^{\kappa}(\theta,\phi)\kappa_{11} + F_{12}^{\kappa}(\theta,\phi)\kappa_{12} + F_{22}^{\kappa}(\theta,\phi)\kappa_{22} + F_{1111}^{\beta}(\theta,\phi)\beta_{1111} + F_{1112}^{\beta}(\theta,\phi)\beta_{1112} + F_{1122}^{\beta}(\theta,\phi)\beta_{1122} + F_{1222}^{\beta}(\theta,\phi)\beta_{1222} + F_{2222}^{\beta}(\theta,\phi)\beta_{2222}. \quad (23)$$

It should be noted that in equation 23, the second term in the right-hand side is only a function of offset because the background is VTI, which does not depend on the azimuth. Equations for sensitivities F_{ij} and F_{ijkl} are given in Appendix C.

INVERSION

In this section, the accuracy of inversion for the components of the fracture matrices from synthetic AVOA data is examined. Synthetic PP-reflection data were calculated using equation 22 (with known elastic parameters), and random noise was added. The fractured medium was assumed to have monoclinic symmetry with two vertical asymmetric fracture sets having azimuths of −30° and 50° with respect to the x_1-direction. The fracture sets had different fracture densities, with 70% of the contribution to the trace of α_{ij} coming from one set, and 30% from the other set. Fracture compliances gave an overall 10% vertical shear-wave splitting if all fractures were parallel. For the examples considered here (gas shale), wide azimuth (WAZ) seismic data were considered with ϕ varying from 0° to 90°. The input to the inversion was the synthetic AVOA data; it is outside the scope of this work to deduce this reflectivity from the amplitudes of received data, as a function of offset, the deduction of which involves many issues (e.g., propagation effects) not considered here.

Depending on the extent of the reservoir and/or fractured area, and also the survey design geometry, one can stack the seismic data in different azimuth and offset intervals to give an increase in fold and signal-to-noise ratio (S/N) as required. (Stacking should be done if the fractures are present in a large area of the reservoir; otherwise, stacking will smear the effect of fractures.) In this work, reflectivity data were assumed to be sparse in azimuth (they are assumed to be stacked in intervals of 5°). Therefore, high-quality reflection data are assumed to be available at 5° steps in azimuth and 2° steps in the offset direction.

For reservoirs with published data in the literature, results of inversion using reflectivity data with S/N = 2 are shown below. Far et al. (2012) analyzed the effect of uncertainty in background elastic parameters. We assume that $B_N/B_T = 0.75$ (which is a reasonable value for gas shales — Sayers and Kachanov, 1995), and that $B_S/B_T = 0.5$. Parameters given by Shan et al. (2010) and Bayuk et al. (2009) for Woodford shale, listed in Table 1, are used (see Far et al. [2012] for more details about parameter selection). The symmetries of the upper and the middle Woodford are shown in Figure 4.

Table 1. Parameters for Woodford shale (Bayuk et al., 2009; Shan et al., 2010).

Woodford shale	V_{P0} (km/s)	V_{S0} (km/s)	Density (g/cm^3)	ε	δ	γ
Upper	4.509	2.855	2.855	0.1	0.1	0.1
Middle	4.161	2.687	2.46	0.29	0.17	0.1

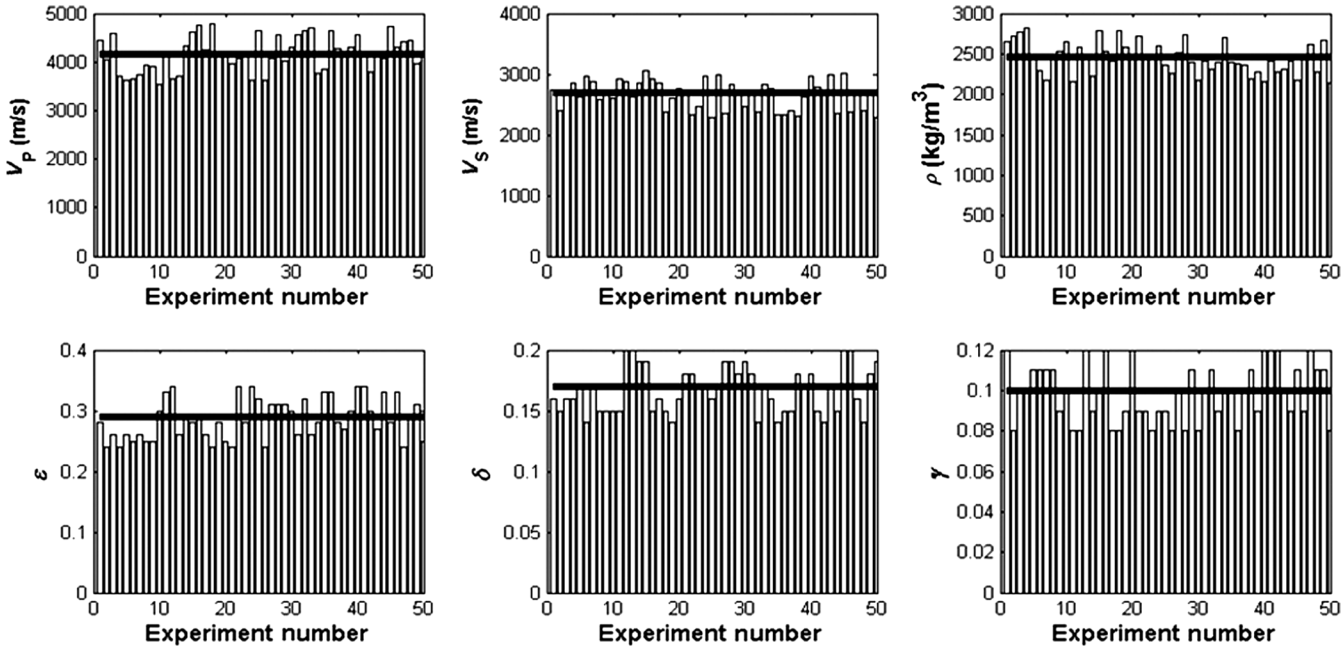

Figure 5. Distributions of randomly generated V_P, V_S, ρ, and Thomsen parameters for Monte Carlo simulation. Horizontal black lines show the values of parameters used for reflectivity modeling.

The forward problem has the following simple form:

$$\mathbf{R} = \mathbf{F}\mathbf{w}. \tag{24}$$

In matrix form,

$$\begin{bmatrix} R_1 \\ R_2 \\ \vdots \\ R_N \end{bmatrix} = \begin{bmatrix} F^{\alpha}_{11_1} & F^{\alpha}_{12_1} & F^{\alpha}_{22_1} & \cdots & F^{\beta}_{2222_1} \\ F^{\alpha}_{11_2} & F^{\alpha}_{12_2} & F^{\alpha}_{22_2} & \cdots & F^{\beta}_{2222_2} \\ \vdots & \vdots & \vdots & \vdots & \vdots \\ F^{\alpha}_{11_N} & F^{\alpha}_{12_N} & F^{\alpha}_{22_N} & \cdots & F^{\beta}_{2222_N} \end{bmatrix} \begin{bmatrix} \alpha_{11} \\ \alpha_{12} \\ \vdots \\ \beta_{2222} \end{bmatrix}, \tag{25}$$

where $\mathbf{R}$ is a vector (of length N) containing all data (reflection coefficients), $\mathbf{w}$ is a vector (of length M) that represents the medium parameters (components of the second- and fourth-rank fracture matrices), and $\mathbf{F}$ is the sensitivity matrix ($N \times M$). Inversion can be performed using the conjugate gradient method.

The background (unfractured) parameters (assumed to be known in this work) can be obtained, with uncertainty, using, e.g., statistical methods (e.g., Eftekharifar and Han, 2011; Far, 2011). Therefore, to invert for fracture parameters using this work, elastic parameters of the background medium without fractures (in our case, VTI parameters of the background medium as shown in Table 1) should be well known (albeit with some uncertainty). To account for the uncertainties in the prediction of background properties, Monte Carlo simulation is used. Thus, "correct" synthetic reflection data (shown by $\mathbf{R}$ in equation 24 above) were computed using the V_P, V_S, ρ, and Thomsen parameters from Table 1. Then 50 sets of randomly and independently generated V_P, V_S, ρ, and Thomsen parameters, with standard deviation equal to 15% of the reservoir elastic parameters (see Figure 5), were used to compute the "incorrect" coefficient matrices contained in $\mathbf{F}$ (equation 24 above). Inversion is performed 50 times in each example, using the correct reflection data and 50 incorrect coefficient matrices. In this way, uncertainty is included in the matrix of coefficients or sensitivities. The black lines show the value of the constant parameters used for forward modeling.

Inversion should be preceded by a resolution matrix analysis (Menke, 1989; Eftekharifar and Sayers, 2011a, 2011b; Far, 2011; Far et al., 2012) to determine the confidence in the inversion for the fracture tensor components.

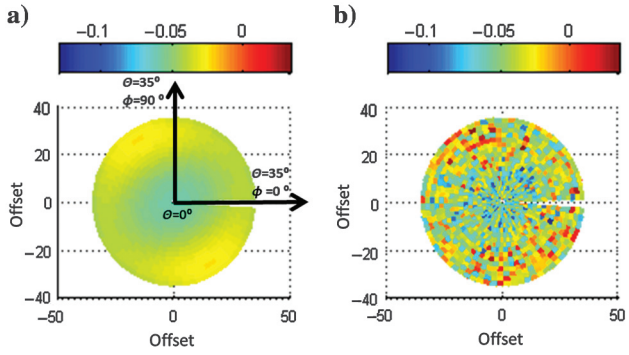

Figure 6. Reflection coefficient plots for WAZ case showing (a) noise free reflectivity and (b) noisy reflectivity with S/N = 2, which was used for inversion.

RESULTS

In this work, two inversion cases are considered: (1) Inversion for asymmetric fracture parameters using WAZ data forward-modeled using the theory of such fractures and (2) inversion for *rotationally invariant* fracture parameters using WAZ data forward-modeled using theory of *asymmetric* fractures. This will be useful to show

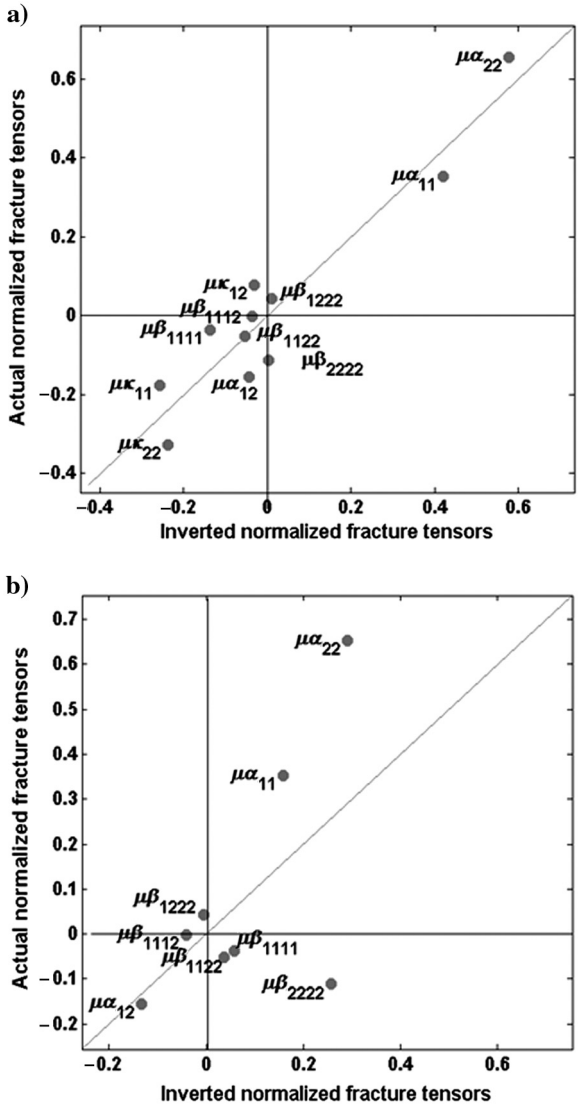

Figure 7. Inversion results for α_{ij}, κ_{ij}, and β_{ijkl} using synthetic WAZ reflectivity data computed with the theory of asymmetric fractures (S/N = 2). (a) Inversion of asymmetric fracture parameters (correlation coefficient = 94%). (b) Inversion of fracture with rotationally *invariant* fracture compliances (correlation coefficient = 75%). In both cases, the fracture compliance matrix components values are made dimensionless by multiplying by the shear modulus of the background medium. The vertical axes show the components of the fracture compliance matrices computed by forward modeling, and the horizontal axes show the values obtained from inversion. The comparison of these two figures reveals the importance of our assumptions about fracture shape. As shown in the lower figure, inverting reflectivity data acquired from a fractured medium with asymmetric fractures will yield erroneous results for fracture parameters, if the data are inverted for rotationally invariant fracture parameters.

the effects of incorrect assumptions about fractures on the inversion results.

Modeled WAZ reflectivity data are shown in Figure 6a. Noisy reflectivity with S/N = 2, which was used for inversion, is shown in Figure 6b. Inversion results for the two cases discussed above (assuming that the background unfractured rock properties are known exactly) are shown in Figure 7. Figure 7a shows the inversion results for asymmetric fracture parameters using reflectivity data computed with the theory of such fractures (S/N = 2). Figure 7b shows the results of inversion for the fracture compliance matrices using the same reflectivity data as used in the upper figure, but with the assumption that fractures have rotationally *invariant* shear compliance (wrong assumption). Successful inversion of a particular matrix component is indicated by a small departure from the diagonal line (perfect inversion), compared to the distance from the origin. By this measure, many of the components in case 1 (Figure 7a) are successfully inverted. However, in case 2 (Figure 7b), the incorrect assumption of fracture symmetry introduces large errors in prediction of most $\boldsymbol{\alpha}$ and $\boldsymbol{\beta}$ components.

Figure 8 shows the results of inversion (Monte Carlo simulation) for the components of the compliance matrices and also for the direction of the fast-shear-wave polarization, when there is a 15% uncertainty in the background unfractured rock properties. This figure shows the results of inversion of asymmetric fracture parameters using noisy WAZ data forward-modeled using the theory of asymmetric fractures. Where the various experiments show large variation, it follows that any conclusion concerning that AVOA parameter is critically dependent on uncertainty in the (azimuthally isotropic) background parameters. This is the case for most of the fracture compliance components, although the direction of fast-shear-wave polarization is robust. It seems intuitively clear that this direction is closely related to the direction of maximum hydraulic permeability.

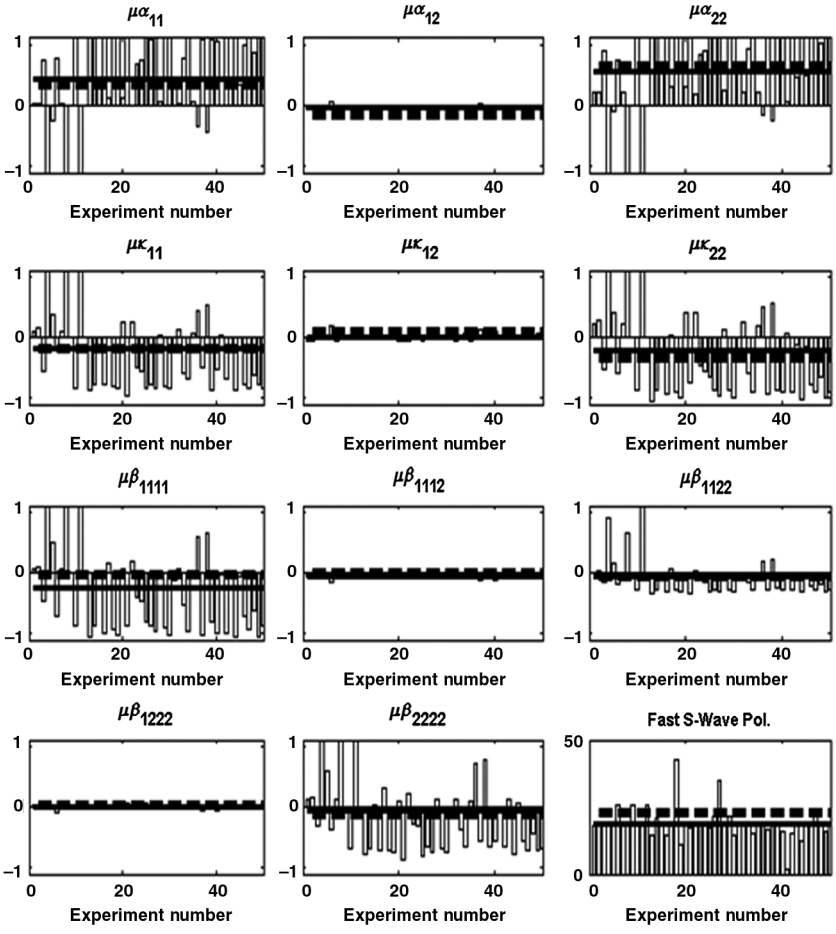

Figure 8. Monte Carlo simulation results using synthetic WAZ data (asymmetric fractures) with S/N = 2. Dashed lines show the actual values of the fracture compliance matrix components obtained by forward modeling, and thin solid lines show the average values obtained from 50 inversions. The components of the fracture compliance matrices are made dimensionless by multiplying by the shear modulus of the background medium. The vertical axes show the magnitude of the components of dimensionless fracture compliance matrices, clipped at ±1 (for the fast-shear-wave polarization plot, the vertical axes show the direction of polarization in degrees). The horizontal axes show the experiment number.

CONCLUSIONS

In this work, a theory for modeling reservoirs with arbitrary number of vertical asymmetric fracture sets is developed and tested by inversion of synthetic PP AVOA data that requires no a priori knowledge about fracture orientations. It was shown that if the parameters defining the VTI background are known, then several components of matrices that describe fracture properties, for media with monoclinic or orthorhombic symmetry (which can take into account the VTI background and multiple fracture sets), can be inverted reliably. If the parameters defining the background are uncertain, the reliability of the fracture parameters obtained by inversion is reduced significantly. However, a reliable estimation of the principal axes appears possible.

The previous approach that considered rotationally invariant fractures, was generalized for rotationally varying (asymmetric) vertical fractures. This generalization introduces another second-rank tensor, κ_{ij}, the magnitude of which is directly related to the asymmetry of the fractures.

Because the elastic properties of background media without fractures do not cause azimuthal changes in AVOA data, due to the different nature of these properties compared to components of the fracture compliance matrices (which cause azimuthal anomalies), simultaneous inversion for these two different properties requires further constraints.

This work does not require a priori knowledge about the number and the direction of fracture sets. After inversion, nothing can be said about the number of fracture sets and the direction of individual fracture sets without further assumptions. However, inversion results for the fracture tensors give the most compliant orientation in the fractured medium. If there is a priori knowledge about the number of fracture sets, one might be able to predict the fracture orientations. As an example, if we know there is one set of

fractures in the reservoir, in theory, their direction can be inverted uniquely.

ACKNOWLEDGMENTS

The first author thanks D. Han for providing useful background information and financial support via the Fluid and DHI Consortium at the University of Houston and for many useful comments and suggestions.

APPENDIX A

ARBITRARILY ORIENTED ASYMMETRIC FRACTURES

Following and extending Kachanov (1992), the fracture compliance matrix for a planar fracture with normal **n** and principal axes **s** and **t** in the plane of the fracture can be written as

$$\mathbf{B} = B_N \mathbf{nn} + B_S \mathbf{ss} + B_T \mathbf{tt}, \tag{A-1}$$

where **s** and **t** are unit vectors in the principal directions in the fracture plane. In component form,

$$B_{ij} = B_N n_i n_j + B_S s_i s_j + B_T t_i t_j. \tag{A-2}$$

The previous treatment, described above in this paper, is limited to vertical fractures, because these constitute a large fraction of the cases of interest, and the algebra is simpler than the general case. Here we treat the general case. To find the general form of the additional compliance when fractures are not aligned with any of the coordinate axes (see Figure A-1), one can use tensor rotation (or Bond transformation) with Euler angles θ around the y-axis, followed by a ϕ rotation around the new z-axis.

Using the method of Sayers and Kachanov (1995), the contribution ΔS_{ijkl} of the fractures to the elastic compliance S_{ijkl} is given by

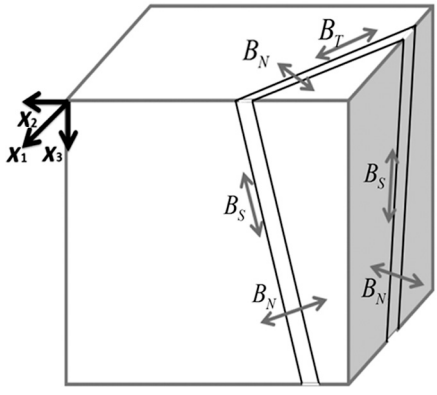

Figure A-1. General situation for an asymmetric fracture in which the fracture is not aligned with any of the coordinate axes.

$$\Delta S_{ijkl} = \frac{1}{V}\sum_r \Big[B_N^{(r)} n_i^{(r)} n_j^{(r)} n_k^{(r)} n_l^{(r)} + \frac{B_S^{(r)}}{4}(s_i^{(r)} s_k^{(r)} n_j^{(r)} n_l^{(r)} + s_i^{(r)} s_l^{(r)} n_j^{(r)} n_k^{(r)} + s_j^{(r)} s_k^{(r)} n_i^{(r)} n_l^{(r)} + s_j^{(r)} s_l^{(r)} n_i^{(r)} n_k^{(r)}) + \frac{B_T^{(r)}}{4}(t_i^{(r)} t_k^{(r)} n_j^{(r)} n_l^{(r)} + t_i^{(r)} t_l^{(r)} n_j^{(r)} n_k^{(r)} + t_j^{(r)} t_k^{(r)} n_i^{(r)} n_l^{(r)} + t_j^{(r)} t_l^{(r)} n_i^{(r)} n_k^{(r)}) \Big] A^{(r)}. \tag{A-3}$$

Using the identity $\mathbf{nn} + \mathbf{ss} + \mathbf{tt} = \mathbf{I}$, equation A-3 can be written as

$$\Delta S_{ijkl} = \frac{1}{V}\sum_r \Big[(B_N^{(r)} - B_T^{(r)}) n_i^{(r)} n_j^{(r)} n_k^{(r)} n_l^{(r)} + \frac{(B_S^{(r)} - B_T^{(r)})}{4}(s_i^{(r)} s_k^{(r)} n_j^{(r)} n_l^{(r)} + s_i^{(r)} s_l^{(r)} n_j^{(r)} n_k^{(r)} + s_j^{(r)} s_k^{(r)} n_i^{(r)} n_l^{(r)} + s_j^{(r)} s_l^{(r)} n_i^{(r)} n_k^{(r)}) + \frac{B_T^{(r)}}{4}(\delta_{ik} n_j^{(r)} n_l^{(r)} + \delta_{il} n_j^{(r)} n_k^{(r)} + \delta_{jk} n_i^{(r)} n_l^{(r)} + \delta_{jl} n_i^{(r)} n_k^{(r)}) \Big] A^{(r)}. \tag{A-4}$$

APPENDIX B

GENERALIZED ANISOTROPY PARAMETERS

In terms of the specific compliance matrices, generalized anisotropy parameters are defined as below (Far et al., 2012). It should be noted that in these equations, C_{ij} are the components of the stiffness matrix of the VTI background (unfractured rock):

$$\varepsilon_x = \varepsilon + \frac{-C_{11}^2(\alpha_{11} + \beta_{1111}) - C_{12}^2(\alpha_{22} + \beta_{2222}) - 2C_{11}C_{12}\beta_{1122}}{2C_{33}}, \tag{B-1}$$

$$\varepsilon_y = \varepsilon + \frac{-C_{12}^2(\alpha_{11} + \beta_{1111}) - C_{11}^2(\alpha_{22} + \beta_{2222}) - 2C_{11}C_{12}\beta_{1122}}{2C_{33}}, \tag{B-2}$$

$$\varepsilon_z = \frac{-C_{13}^2(\alpha_{11} + \beta_{1111} + \alpha_{22} + \beta_{2222} + 2\beta_{1122})}{2C_{33}}, \tag{B-3}$$

$$\varepsilon_{16} = -\frac{C_{66}(2C_{11}\beta_{1112} + 2C_{12}\beta_{1222} + \alpha_{12}(C_{11} + C_{12}))}{C_{33}}, \tag{B-4}$$

$$\varepsilon_{26} = -\frac{C_{66}(2C_{12}\beta_{1112} + 2C_{11}\beta_{1222} + \alpha_{12}(C_{11} + C_{12}))}{C_{33}}, \tag{B-5}$$

$$\varepsilon_{45} = \frac{-C_{45}^2(\alpha_{12}+\kappa_{12})}{C_{55}}, \tag{B-6}$$

$$\delta_x = \delta^w + \frac{-C_{13}[C_{11}(\alpha_{11}+\beta_{1111})+C_{12}(\alpha_{22}+\beta_{2222})+\beta_{1122}(C_{11}+C_{12})]-2C_{55}^2(\alpha_{11}+\kappa_{11})}{C_{33}}, \tag{B-7}$$

$$\delta_y = \delta^w + \frac{-C_{13}[C_{12}(\alpha_{11}+\beta_{1111})+C_{11}(\alpha_{22}+\beta_{2222})+\beta_{1122}(C_{11}+C_{12})]-2C_{55}^2(\alpha_{22}+\kappa_{22})}{C_{33}}, \tag{B-8}$$

$$\delta_z = 2\varepsilon + \frac{C_{11}C_{12}(\alpha_{11}+\beta_{1111}+\alpha_{22}+\beta_{2222})-\beta_{1122}(C_{11}+C_{12})-2C_{66}^2(\alpha_{11}+\alpha_{22}+4\beta_{1122})}{C_{33}}, \tag{B-9}$$

$$\gamma_x = -\frac{C_{55}(\alpha_{11}+\kappa_{11})}{2}, \tag{B-10}$$

$$\gamma_y = -\frac{C_{55}(\alpha_{22}+\kappa_{22})}{2}, \tag{B-11}$$

$$\chi_z = \frac{-2C_{66}C_{13}(\alpha_{12}+\beta_{1112}+\beta_{1222})-2C_{55}^2(\alpha_{12}+\kappa_{12})}{C_{33}}. \tag{B-12}$$

APPENDIX C

SENSITIVITY EQUATIONS

Equation 22 can be rewritten by collecting the terms that are multiplied by each of the fracture parameters. This is done by keeping one fracture parameter (components of $\boldsymbol{\alpha}$, $\boldsymbol{\kappa}$, and $\boldsymbol{\beta}$) at a time and zeroing out the other parameters and collecting the terms that are multiplied by that nonzero parameter. These sets of coefficients (F_{ijkl} or F_{ij}) are called sensitivities. Sensitivities in equation 23 obtained as

$$F_{11}^{\alpha}(\theta,\phi) = \frac{1}{\mu}\left[-\frac{C_{13}^2}{4C_{33}} + \left(\frac{C_{13}^2}{2C_{33}} + \left(\frac{4C_{55}\bar{V}_S^2}{\bar{V}_P^2} - \frac{2C_{55}^2 + C_{11}C_{13}}{C_{33}}\right)\cos^2(\phi) - \frac{C_{12}C_{13}\sin^2(\phi)}{C_{33}}\right)\frac{1}{2}\sin^2(\theta) + \left(-\frac{C_{12}^2\sin^4(\phi) + C_{11}^2\cos^4(\phi) + (C_{11}^2+C_{12}^2)\sin^2(\phi)\cos^2(\phi)}{2C_{33}}\right) \times\frac{1}{2}\sin^2(\theta)\tan^2(\theta)\right], \tag{C-1}$$

$$F_{12}^{\alpha}(\theta,\phi) = \frac{1}{\mu}\left[\left(\frac{4C_{55}\bar{V}_S^2}{\bar{V}_P^2} - \frac{2C_{55}^2 + 2C_{13}C_{66}}{C_{33}}\right)\sin(\phi)\cos(\phi)\sin^2(\theta) + \left(-\frac{(C_{11}+C_{12})C_{66}}{C_{33}}\right)\sin(\phi)\cos(\phi)\sin^2(\theta)\tan^2(\theta)\right], \tag{C-2}$$

$$F_{22}^{\alpha}(\theta,\phi) = \frac{1}{\mu}\left[-\frac{C_{13}^2}{4C_{33}} + \left(\frac{C_{13}^2}{2C_{33}} - \frac{C_{12}C_{13}}{C_{33}}\left(\frac{4C_{55}\bar{V}_S^2}{\bar{V}_P^2} + \frac{-C_{11}C_{13}-C_{55}^2}{C_{33}}\right)\cos^2(\phi)\right) \times\frac{1}{2}\sin^2(\phi)\sin^2(\theta) + \left(-\frac{C_{12}^2\sin^4(\phi) + C_{11}^2\cos^4(\phi) + (C_{11}^2+C_{12}^2)\sin^2(\phi)\cos^2(\phi)}{2C_{33}}\right) \times\frac{1}{2}\sin^2(\theta)\tan^2(\theta)\right], \tag{C-3}$$

$$F_{11}^{\kappa}(\theta,\phi) = \frac{1}{\mu}\left[\frac{1}{2}\left(\frac{4C_{55}\bar{V}_S^2}{\bar{V}_P^2} - \frac{2C_{55}^2}{C_{33}}\right)\sin^2(\theta)\cos^2(\phi)\right], \tag{C-4}$$

$$F_{12}^{\kappa}(\theta,\phi) = \frac{1}{\mu}\left[\left(\frac{4C_{55}\bar{V}_S^2}{\bar{V}_P^2} - \frac{2C_{55}^2}{C_{33}}\right)\sin(\phi)\cos(\phi)\sin^2(\theta)\right], \tag{C-5}$$

$$F_{22}^{\kappa}(\theta,\phi) = \frac{1}{\mu}\left[\frac{1}{2}\left(\frac{4C_{55}\bar{V}_S^2}{\bar{V}_P^2} + \frac{-2C_{55}^2}{C_{33}}\right)\sin^2(\phi)\sin^2(\theta)\right], \tag{C-6}$$

$$F_{1111}^{\beta}(\theta,\phi) = \frac{1}{\mu}\left[-\frac{C_{13}^2}{4C_{33}} + \frac{1}{2}\left(\frac{C_{13}^2}{2C_{33}} - \frac{C_{12}C_{13}\sin^2(\phi)}{C_{33}} - \frac{C_{11}C_{13}\cos^2(\phi)}{C_{33}}\right)\sin^2(\theta) - \frac{1}{2}\left(\frac{(C_{11}\cos^2(\phi)+C_{12}\sin^2(\phi))^2}{2C_{33}}\right) \times\sin^2(\theta)\tan^2(\theta)\right], \tag{C-7}$$

$$F_{1112}^{\beta}(\theta,\phi) = \frac{1}{\mu}\left[\left(-\frac{2C_{66}(C_{12}\sin^2(\phi)+C_{11}\cos^2(\phi))}{C_{33}}\right) \times\sin(\phi)\cos(\phi)\sin^2(\theta)\tan^2(\theta) - \frac{2C_{13}C_{66}}{C_{33}}\sin(\phi)\cos(\phi)\sin^2(\theta)\right], \tag{C-8}$$

$$F_{1122}^{\beta}(\theta,\phi) = \frac{1}{\mu}\left[-\frac{C_{13}^2}{2C_{33}} - \frac{1}{2}\left(\frac{C_{13}(C_{11}+C_{12}-C_{13})}{C_{33}}\right)\sin^2(\theta) + \left(-\frac{C_{11}C_{12}(\sin^4(\phi)+\cos^4(\phi)-4\sin^2(\phi)\cos^2(\phi))+3(C_{11}^2+C_{12}^2)}{C_{33}}\right) \times\frac{1}{2}\sin^2(\theta)\tan^2(\theta)\right], \tag{C-9}$$

$$F_{1222}^{\beta}(\theta,\phi) = \frac{1}{\mu}\left[-\frac{2C_{13}C_{66}}{C_{33}}\sin(\phi)\cos(\phi)\sin^2(\theta) + \left(-\frac{2C_{66}(C_{11}\sin^2(\phi)+C_{12}\cos^2(\phi))}{C_{33}}\right) \times\sin(\phi)\cos(\phi)\sin^2(\theta)\tan^2(\theta)\right], \tag{C-10}$$

$$F^{\beta}_{2222}(\theta,\phi) = \frac{1}{\mu}\left[-\frac{C_{13}^2}{4C_{33}} + \frac{1}{2}\left(-\frac{C_{11}C_{13}\sin^2(\phi)}{C_{33}} - \frac{C_{12}C_{13}\cos^2(\phi)}{C_{33}} + \frac{C_{13}^2}{2C_{33}}\right)\sin^2(\theta) + \frac{1}{2}\left(-\frac{(C_{12}\cos^2(\phi) + C_{11}\sin^2(\phi))^2}{2C_{33}}\right) \times \sin^2(\theta)\tan^2(\theta)\right]. \quad \text{(C-11)}$$

REFERENCES

Bakulin, A. V., V. Grechka, and I. Tsvankin, 2000, Estimation of fracture parameters from reflection seismic data. Part III: Fractured models with monoclinic symmetry: Geophysics, **65**, 1818–1830, doi: 10.1190/1.1444865.

Bayuk, I. O., E. Chesnokov, M. Ammermann, and N. Dyaur, 2009, Elastic properties of four shales reconstructed from laboratory measurements at unloaded conditions: 79th Annual International Meeting, SEG, Expanded Abstracts, 2634–2638.

Budiansky, B., and R. J. O'Connell, 1976, Elastic moduli of a cracked solid: International Journal of Solids and Structures, **12**, 81–97, doi: 10.1016/0020-7683(76)90044-5.

Eftekharifar, E., and D.-H. Han, 2011, 3D petrophysical modeling using complex seismic attributes and limited well log data: 81st Annual International Meeting, SEG, Expanded Abstracts, 1887–1891.

Eftekharifar, M., and C. M. Sayers, 2011a, Seismic characterization of fractured reservoirs: A resolution matrix approach: 81st Annual International Meeting, SEG, Expanded Abstracts, 1953–1957.

Eftekharifar, M., and C. M. Sayers, 2011b, Seismic characterization of fractured reservoirs: Inversion for fracture parameters illustrated using synthetic AVOA data: 81st Annual International Meeting, SEG, Expanded Abstracts, 370–374.

Far, M. E., 2011, Seismic characterization of naturally fractured reservoirs: Ph.D. dissertation, University of Houston.

Far, M. E., C. M. Sayers, L. Thomsen, D. Han, and J. P. Castagna, 2013, Seismic characterization of naturally fractured reservoirs using amplitude versus offset and azimuth analysis: Geophysical Prospecting, doi: 10.1111/1365-2478.12011.

Far, M. E., L. Thomsen, and C. M. Sayers, 2012, Inversion for asymmetric fracture parameters using synthetic AVOA data: 82nd Annual International Meeting, SEG, Expanded Abstracts, 1–5.

Helbig, K., 1994, Foundations of elastic anisotropy for exploration seismics: Pergamon Press.

Hill, R., 1963, Elastic properties of reinforced solids: Some theoretical principles: Journal of the Mechanics and Physics of Solids, **11**, 357–372, doi: 10.1016/0022-5096(63)90036-X.

Jones, J. P., and J. S. Whittier, 1967, Waves at a flexibly bonded interface: Journal of Applied Mechanics, **34**, 905–909, doi: 10.1115/1.3607854.

Kachanov, M., 1980, Continuum model of medium with cracks: Journal of the Engineering Mechanics Division of the American Society of Civil Engineers, **106**, 1039–1051.

Kachanov, M., 1992, Effective elastic properties of cracked solids: Critical review of some basic concepts: Applied Mechanics Reviews, **45**, 304–335, doi: 10.1115/1.3119761.

Lehner, F. K., 2008, Chemomechanics and diagenesis: Pressure solution as example: Presented at the Zu Grundproblemen der Geologie kolloquium: Leibnitz-Sozietät der Wissenschaften zu Berlin.

Lynn, H. B., C. R. Bates, M. Layman, and M. Jones, 1994, Natural fracture characterization using P-wave reflection seismic data, VSP, borehole imaging logs, and in-situ stress field determination: SPE Paper 29595.

Mallick, S., R. E. Chambers, and A. Gonzalez, 1996, Method for determining the principal axes of azimuthal anisotropy from seismic P-wave data: U. S. Patent 5,508,973.

Margetan, F. J., R. B. Thomsen, and T. A. Gray, 1988, Interfacial spring model for ultrasonic interactions with imperfect interfaces: Theory of oblique incidence and application to diffusion-bonded joints: Journal of Nondestructive Evaluation, **7**, 131–152, doi: 10.1007/BF00565998.

Menke, W., 1989, Geophysical data analysis: Discrete inverse theory: Academic Press.

Nichols, D., F. Muir, and M. Schoenberg, 1989, Elastic properties of rocks with multiple sets of fractures: 59th Annual International Meeting, SEG, Expanded Abstracts, 471–474.

Pšenčík, I., and J. L. Martins, 2001, Properties of weak contrast PP reflection/transmission coefficients for weakly anisotropic elastic media: Studia Geophysica et Geodaetica, **45**, 176–199, doi: 10.1023/A:1021868328668.

Rüger, A., 1997, P-wave reflection coefficients for transversely isotropic media with vertical and horizontal axis of symmetry: Geophysics, **62**, 713–722, doi: 10.1190/1.1444181.

Sayers, C. M., 1998, Misalignment of the orientation of fractures and the principal axes for P- and S-waves in rocks containing multiple non-orthogonal fracture sets: Geophysical Journal International, **133**, 459–466, doi: 10.1046/j.1365-246X.1998.00507.x.

Sayers, C. M., 2009, Seismic characterization of reservoirs containing multiple fracture sets: Geophysical Prospecting, **57**, 187–192, doi: 10.1111/j.1365-2478.2008.00766.x.

Sayers, C. M., 2010, Geophysics under stress: Geomechanical applications of seismic and borehole acoustic waves: SEG/EAGE 2010 Distinguished Instructor Short Course, Society of Exploration Geophysicists and European Association of Geoscientists and Engineers.

Sayers, C. M., and S. Dean, 2001, Azimuth-dependent AVO in reservoirs containing non-orthogonal fracture sets: Geophysical Prospecting, **49**, 100–106, doi: 10.1046/j.1365-2478.2001.00236.x.

Sayers, C. M., and M. Kachanov, 1991, A simple technique for finding effective elastic constants of cracked solids for arbitrary crack orientation statistics: International Journal of Solids and Structures, **27**, 671–680, doi: 10.1016/0020-7683(91)90027-D.

Sayers, C. M., and M. Kachanov, 1995, Microcrack-induced elastic wave anisotropy of brittle rocks: Journal of Geophysical Research, **100**, 4149–4156, doi: 10.1029/94JB03134.

Sayers, C. M., and J. E. Rickett, 1997, Azimuthal variation in AVO response for fractured gas sands: Geophysical Prospecting, **45**, 165–182, doi: 10.1046/j.1365-2478.1997.3180238.x.

Schoenberg, M., 1980, Elastic wave behavior across linear slip interfaces: Journal of the Acoustical Society of America, **68**, 1516–1521, doi: 10.1121/1.385077.

Sevostianov, I., and M. Kachanov, 2002, On the elastic compliances of irregularly shaped cracks: International Journal of Fracture, **114**, 245–257, doi: 10.1023/A:1015534127172.

Shan, N., R. Tatham, M. K. Sen, K. Spikes, and S. C. Ruppel, 2010, Sensitivity of seismic response to variations in the Woodford shale: 80th Annual International Meeting, SEG, Expanded Abstracts, 2725–2729.

Sil, S., M. Davidson, C. Zhou, R. Olson, H. Swan, J. Howell, S. Chiu, and M. Willis, 2011, Effect of near-surface anisotropy on a deep anisotropic target layer: 81st Annual International Meeting, SEG, Expanded Abstracts, 305–309.

Tada, H., P. C. Paris, and G. R. Irwin, 1973, The stress analysis of cracks handbook: Dell Research Corporation.

Thomsen, L., 1986, Weak elastic anisotropy: Geophysics, **51**, 1954–1966, doi: 10.1190/1.1442051.

Worthington, M. H., 2008, Interpreting seismic anisotropy in fractured reservoirs: First Break, **26**, 57–63.